Convection and ^{6}Li in the atmospheres of metal-poor halo stars

M. Steffen[1], R. Cayrel[2], P. Bonifacio[2], H.-G. Ludwig[3], E. Caffau[2]

[1]Astrophysiklaisches Institut Potsdam, An der Sternwarte 16, D-14482 Potsdam, Germany

[2]GEPI – Observatoire de Paris, Paris, France

[3]ZAH-Landessternwarte, Königstuhl 12, D-69117 Heidelberg, Germany

Abstract. Based on 3D hydrodynamical model atmospheres computed with the CO^{5}BOLD code and 3D non-LTE (NLTE) line formation calculations, we study the effect of the convection-induced line asymmetry on the derived ^{6}Li abundance for a range in effective temperature, gravity, and metallicity covering the stars of the Asplund *et al.* (2006) sample. When the asymmetry effect is taken into account for this sample of stars, the resulting ^{6}Li/^{7}Li ratios are reduced by about 1.5% on average with respect to the isotopic ratios determined by Asplund *et al.* (2006). This purely theoretical correction diminishes the number of significant ^{6}Li detections from 9 to 4 (2σ criterion), or from 5 to 2 (3σ criterion). In view of this result the existence of a ^{6}Li plateau appears questionable. A careful reanalysis of individual objects by fitting the observed lithium 6707 Å doublet both with 3D NLTE and 1D LTE synthetic line profiles confirms that the inferred ^{6}Li abundance is systematically lower when using 3D NLTE instead of 1D LTE line fitting. Nevertheless, halo stars with unquestionable ^{6}Li detection do exist even if analyzed in 3D-NLTE, the most prominent example being HD 84937.

Keywords. stars: abundances, stars: atmospheres, hydrodynamics, convection, radiative transfer, line: formation, line: profiles, stars: individual (G271-162, HD 74000, HD 84937)

1. Introduction

The spectroscopic signature of the presence of ^{6}Li in the atmospheres of metal-poor halo stars is a subtle extra depression in the red wing of the ^{7}Li doublet, which can only be detected in spectra of the highest quality. Based on high-resolution, high signal-to-noise VLT/UVES spectra of 24 bright metal-poor stars, Asplund *et al.* (2006) report the detection of ^{6}Li in nine of these objects. The average ^{6}Li/^{7}Li isotopic ratio in the nine stars in which ^{6}Li has been detected is about 4% and is very similar in each of these stars, defining a ^{6}Li plateau at approximately $\log n(^6\text{Li}) = 0.85$ (on the scale $\log n(\text{H}) = 12$). A convincing theoretical explanation of this new ^{6}Li plateau turned out to be problematic: the high abundances of ^{6}Li at the lowest metallicities cannot be explained by current models of galactic cosmic-ray production, even if the depletion of ^{6}Li during the pre-main-sequence phase is ignored (see reviews by e.g. Christlieb 2008, Cayrel *et al.* 2008, Prantzos 2010 [this volume] and references therein).

A possible solution of the so-called 'second Lithium problem' was proposed by Cayrel *et al.* (2007), who point out that the intrinsic line asymmetry caused by convection in the photospheres of metal-poor turn-off stars is almost indistinguishable from the asymmetry produced by a weak ^{6}Li blend on a presumed symmetric ^{7}Li profile. As a consequence, the derived ^{6}Li abundance should be significantly reduced when the intrinsic line asymmetry in properly taken into account. Using 3D NLTE line formation calculations based on 3D hydrodynamical model atmospheres computed with the CO^{5}BOLD code (Freytag *et al.* 2002, Wedemeyer *et al.* 2004, see also http://www.astro.uu.se/~bf/co5bold_main.html),

we quantify the theoretical effect of the convection-induced line asymmetry on the resulting ^{6}Li abundance as a function of effective temperature, gravity, and metallicity, for a parameter range that covers the stars of the Asplund *et al.* (2006) sample.

A careful reanalysis of individual objects is under way, in which we consider two alternative approaches for fixing the residual line broadening, $V_{\rm BR}$, the combined effect of macroturbulence (1D only) and instrumental broadening, for given microturbulence (1D only) and rotational velocity: (i) treating $V_{\rm BR}$ as a free parameter when fitting the Li feature, (ii) deriving $V_{\rm BR}$ from additional unblended spectral lines with similar properties as Li I 6707. We show that method (ii) is potentially dangerous, because the inferred broadening parameter shows considerable line-to-line variations, and the resulting ^{6}Li abundance depends rather sensitively on the adopted value of $V_{\rm BR}$.

2. 3D hydrodynamical simulations and spectrum synthesis

The hydrodynamical atmospheres used in the present study are part of the CIFIST 3D model atmosphere grid (Ludwig *et al.* 2009). They have been obtained from realistic numerical simulations with the CO^{5}BOLD code which solves the time-dependent equations of compressible hydrodynamics in a constant gravity field together with the equations of non-local, frequency-dependent radiative transfer in a Cartesian box representative of a volume located at the stellar surface. The computational domain is periodic in x and y direction, has open top and bottom boundaries, and is resolved by typically $140 \times 140 \times 150$ grid cells. The vertical optical depth of the box varies from $\log \tau_{\rm Ross} \approx -8$ (top) to $\log \tau_{\rm Ross} \approx +7.5$ (bottom), and the radiative transfer is solved in 6 or 12 opacity bins. Further information about the models used in the present study is compiled in Table 1. Each of the models is represented by a number of snapshots, indicated in column (6), chosen from the full time sequence of the corresponding simulation.

These representative snapshots are processed by the non-LTE code NLTE3D that solves the statistical equilibrium equations for a 17 level lithium atom with 34 line transitions, fully taking into account the 3D thermal structure of the respective model atmosphere. The photo-ionizing radiation field is computed at 704 frequency points between $\lambda\, 925$ and $32\,407$ Å, using the opacity distribution functions of Castelli & Kurucz (2004) to allow for metallicity-dependent line-blanketing, including the H I–H$^+$ and H I–H I quasi-molecular absorption near $\lambda\, 1400$ and 1600 Å, respectively. Collisional ionization by neutral hydrogen via the charge transfer reaction H$(1s) + Li(n\ell) \leftrightarrow$ Li$^+(1s^2) + H^-$ is treated according to Barklem, *et al.* (2003). More details are given in Sbordone *et al.* (2009). Finally, 3D NLTE synthetic line profiles of the Li I $\lambda\, 6707$ Å doublet are computed with the line formation code Linfor3D (`http://www.aip.de/~mst/linfor3D_main.html`), using the departure coefficients $b_i = n_i({\rm NLTE})/n_i({\rm LTE})$ provided by NLTE3D for each level i of the lithium model atom as a function of geometrical position within the 3D model atmospheres. As demonstrated in Fig. 1, 3D NLTE effects are very important for the metal-poor dwarfs considered here: they strongly reduce the height range of line formation such that the 3D NLTE equivalent width is smaller by roughly a factor 2 compared to 3D LTE. Ironically, the line strength predicted by standard 1D mixing-length models in LTE are close to the results obtained from elaborate 3D NLTE calculations. We note that the half-width of the 3D NLTE line profile, FWHM(NLTE) = 8.5 km/s, is larger by about 10%: FWHM(LTE) = 7.7 and 7.5 km/s, respectively, before and after reducing the Li abundance such that 3D LTE and 3D NLTE equivalent widths agree. This is because 3D LTE profile senses the higher photosphere where both thermal and hydrodynamical velocities are lower. However, the NLTE line profile is significantly less asymmetric than the LTE profile, even if the latter is broadened to the same half-width (Fig. 1, bottom

Table 1. List of models used in the present study. Columns (2)-(6) give effective temperature, surface gravity, metallicity, number of opacity bins used in the radiation hydrodynamics simulation, and number of snapshots selected for spectrum synthesis. The equivalent width of the synthetic 3D non-LTE ^7Li doublet at $\lambda\,6707$ Å, assuming A(Li)=2.2 and no ^6Li, is given in column (7). Columns (8) and (9) show q_a^*(Li) and q_b^*(Li), the $^6Li/^7Li$ isotopic ratio inferred from fitting this 3D non-LTE line profile with two different kinds of 1D profiles, in each case assuming a rotational broadening of $v \sin i = 0.0\,/\,2.0$ km/s, respectively (see text for details).

Model	$T_{\rm eff}$[1)] [**K**]	$\log g$	[**Fe/H**]	**Nbin**	**Nsnap**	$\mathbf{W}$[2)] [mÅ]	$q_a^*=\mathbf{n}(^6\mathbf{Li})/\mathbf{n}(^7\mathbf{Li})$ $\langle$3D$\rangle$ NLTE [%]	$q_b^*=\mathbf{n}(^6\mathbf{Li})/\mathbf{n}(^7\mathbf{Li})$ 1D LTE [%]
d3t59g40mm30n02	5846	4.0	-3.0	6	20	44.9	1.14 / 1.14	**0.88 / 0.88**
d3t59g45mm30n01	5924	4.5	-3.0	6	19	39.9	0.75 / 0.75	**0.63 / 0.64**
d3t63g40mm30n01	6269	4.0	-3.0	6	20	23.9	1.96 / 1.93	**1.86 / 1.83**
d3t63g40mm30n02	6242	4.0	-3.0	12	20	24.1	1.81 / 1.80	**1.63 / 1.62**
d3t63g45mm30n01	6272	4.5	-3.0	6	18	24.3	1.07 / 1.06	**1.02 / 1.00**
d3t65g40mm30n01	6408	4.0	-3.0	6	20	20.0	1.75 / 1.70	**1.70 / 1.66**
d3t65g45mm30n01	6556	4.5	-3.0	6	12	16.4	1.29 / 1.27	**1.25 / 1.22**
d3t59g35mm20n01	5861	3.5	-2.0	6	20	42.8	2.48 / 2.44	**2.02 / 2.01**
d3t59g40mm20n02	5856	4.0	-2.0	6	20	45.2	1.59 / 1.59	**0.96 / 0.98**
d3t59g45mm20n01	5923	4.5	-2.0	6	18	42.3	1.12 / 1.13	**0.45 / 0.46**
d3t63g35mm20n01	6287	3.5	-2.0	6	20	22.1	4.09 / 4.00	**4.04 / 3.97**
d3t63g40mm20n01	6278	4.0	-2.0	6	16	23.7	1.95 / 1.94	**1.79 / 1.78**
d3t63g40mm20n02	6215	4.0	-2.0	12	20	25.1	1.92 / 1.92	**1.66 / 1.67**
d3t63g45mm20n01	6323	4.5	-2.0	6	19	23.0	1.18 / 1.18	**0.97 / 0.97**
d3t65g40mm20n01	6534	4.0	-2.0	6	19	16.2	2.28 / 2.21	**2.22 / 2.16**
d3t65g45mm20n01	6533	4.5	-2.0	6	19	17.0	1.31 / 1.29	**1.21 / 1.19**
d3t59g40mm10n02	5850	4.0	-1.0	6	20	41.5	1.60 / 1.62	**1.45 / 1.47**
d3t59g45mm10n01	5923	4.5	-1.0	6	08	38.2	1.14 / 1.15	**0.83 / 0.85**
d3t63g40mm10n01	6261	4.0	-1.0	6	20	22.0	2.37 / 2.38	**2.33 / 2.33**
d3t63g40mm10n02	6236	4.0	-1.0	12	20	21.8	2.15 / 2.16	**2.05 / 2.06**
d3t63g45mm10n01	6238	4.5	-1.0	6	20	23.4	1.36 / 1.37	**1.23 / 1.24**
d3t65g40mm10n01	6503	4.0	-1.0	6	20	15.5	3.10 / 3.02	**3.14 / 3.06**
d3t65g45mm10n01	6456	4.5	-1.0	6	19	17.1	1.51 / 1.51	**1.44 / 1.43**

*Notes:* [1)] averaged over selected snapshots; [2)] averaged over selected 3D non-LTE spectra

panel).

3. ^{6}Li bias due to convective line asymmetry

As outlined above, the ^{6}Li abundance is systematically overestimated if one ignores the intrinsic asymmetry of the ^{7}Li line components. To quantify this bias theoretically, we rely on synthetic spectra. The idea is as follows: we represent the observation by the synthetic 3D NLTE line profile of the ^{7}Li line blend, computed with zero ^{6}Li content. Except for an optional rotational broadening, the only source of non-thermal line broadening is the 3D hydrodynamical velocity field, which also gives rise to a convective blue-shift and an intrinsic line asymmetry. Now this 3D ^{7}Li line blend is fitted by 'classical' 1D synthetic line profiles composed of intrinsically symmetric components of ^{6}Li and ^{7}Li. Four parameters are varied independently to find the best fit (minimum χ^2): in addition to the total ^{6}Li+^{7}Li abundance, A(Li), and the ^{6}Li/^{7}Li isotopic ratio, q(Li), which control line strength and line asymmetry, respectively, we also allow for a residual line broadening described by a Gaussian kernel with half-width $V_{\rm BR}$, and a global line shift, Δv. Note that the four fitting parameters are non-degenerate, since each one has a distinctly different effect on the line profile. The rotational line broadening is fixed to the value used in the 3D spectrum synthesis (we tried $v \sin i = 0$ and 2 km/s). The value q^*(Li) of the best fit is then identified with the correction that has to be *subtracted* from the ^{6}Li/^{7}Li isotopic ratio derived from the 1D analysis to correct for the bias introduced by neglecting the
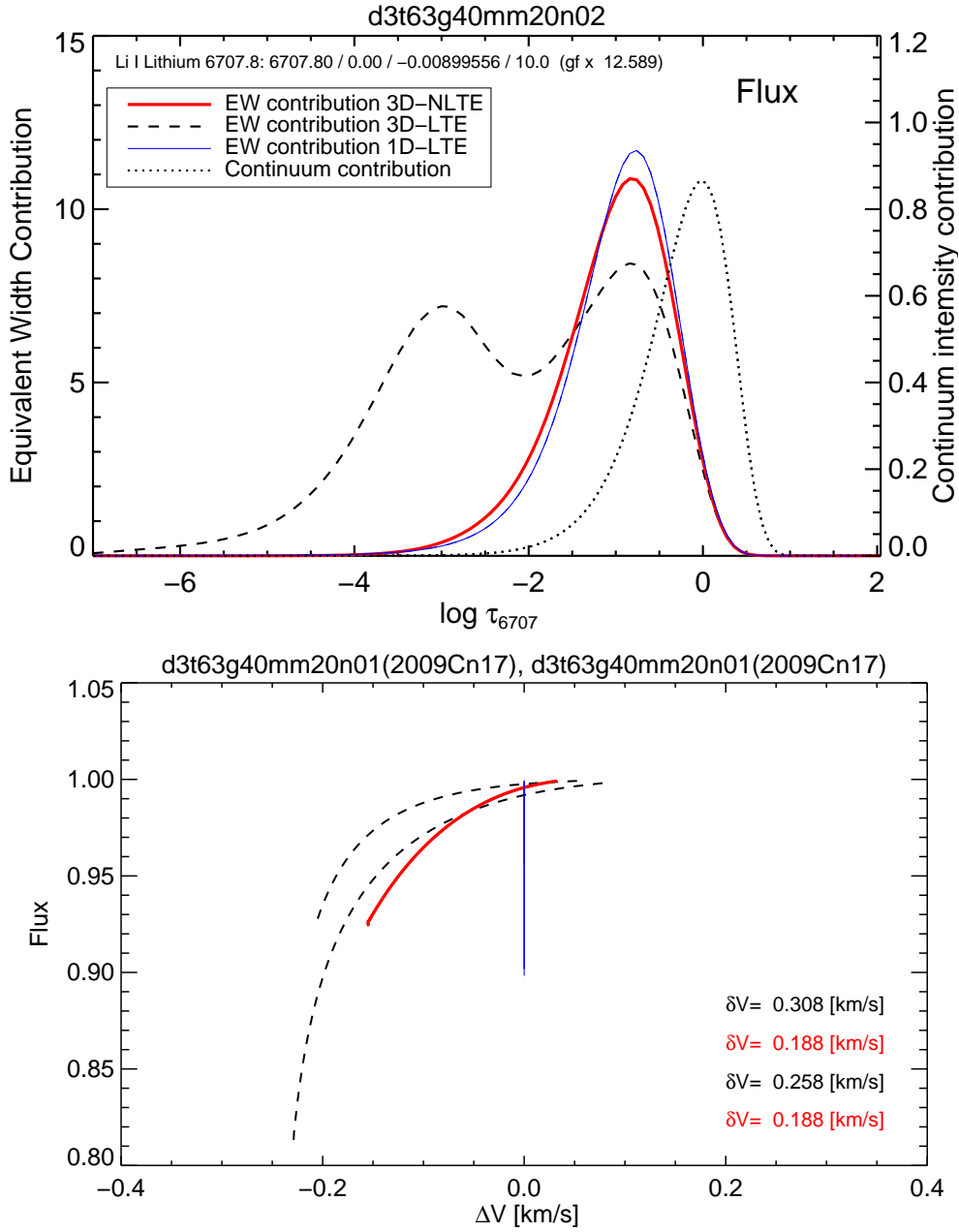
Figure 1. Comparison of 3D LTE (dashed), 3D non-LTE (thick solid), and 1D LTE (thin solid) equivalent width contribution functions (top) and line bisectors (bottom) of a single ^{7}Li component, computed for a typical metal-poor turn-off halo star ($T_{\rm eff} = 6215$ K, $\log g = 4.0$, [Fe/H] $= -2$). Non-LTE effects strongly reduce the height range of formation and equivalent width of the line (W: $35.5 \rightarrow 15.6$ mÅ), while differences between 1D LTE and 3D NLTE are much smaller. The line asymmetry is smaller in non-LTE: the velocity span of the bisector is $\delta v(\rm NLTE) \approx 190$ m/s, while $\delta v(\rm LTE) \approx 310$ and 260 m/s, respectively, before and after adjusting the equivalent width (by reducing the Li abundance) and the half-width (by Gaussian broadening) of the LTE line to match the values of the NLTE profile (compare the two dashed bisectors).
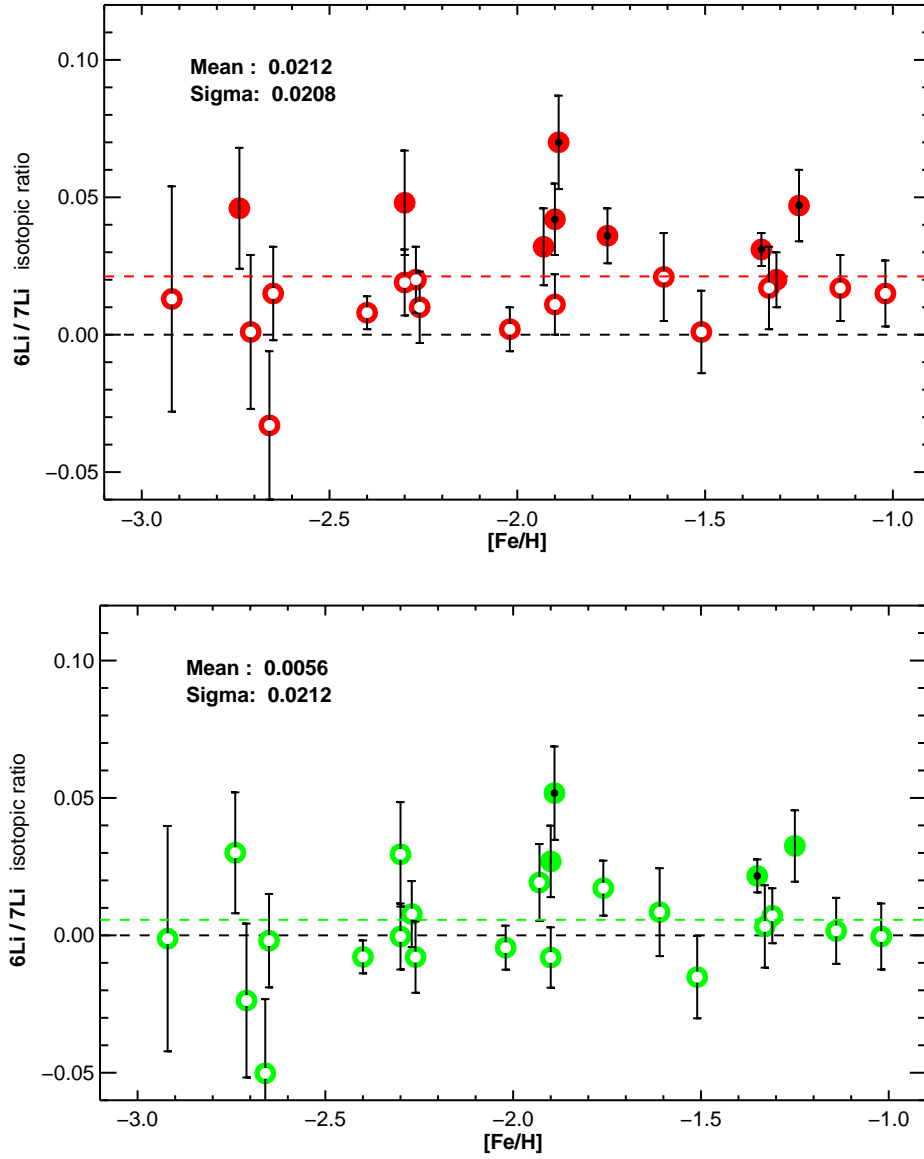
Figure 2. $^6Li/^7Li$ isotopic ratio, and $\pm 1\sigma$ error bars, as a function of metallicity as derived by Asplund *et al.* (2006) before (top) and after (bottom) subtraction of $q_b^*(Li)$ (Table 1, col. (9)) to correct for the bias due to the intrinsic line asymmetry. Open circles denote non-detections, filled circles and filled circles with a black dot denote ^6Li detections above the 2σ and 3σ level, respectively.

intrinsic line asymmetry: $q^{(3D)}(Li) = q^{(1D)}(Li) - q^*(Li)$. The procedure properly accounts for radiative transfer in the lines, including saturation effects.

Two different sets of 1D profiles were used for this purpose: (a) NLTE line profiles based on the $\langle 3D \rangle$ model, constructed by averaging the 3D model on surfaces of constant optical depth, and (b) LTE line profiles computed from a so-called LHD model, a 1D mixing-length model atmosphere that has the same stellar parameters and uses the same

microphysics and radiative transfer scheme as the corresponding 3D model. For both kind of 1D models, the microturbulence was fixed at $\xi_{mic} = 1.5$ km/s. The mixing length parameter adopted for the LHD models is $\alpha_{MLT} = 0.5$.

We have determined $q^*(Li)$ according to the method outlined above for our grid of 3D model atmospheres. The results are given in Table 1, both for fitting with the $\langle 3D \rangle$ NLTE profiles ($q_a^*(Li)$, col. (8)) and with the 1D LTE profiles of the LHD models ($q_b^*(Li)$, col. (9)). At given metallicity, the corrections are largest for low gravity and high effective temperature. They increase towards higher metallicity. We also note that $q^*(Li)$ is essentially insensitive to the choice of the rotational broadening.

The analysis of Asplund *et al.* (2006) utilizes 1D LTE profiles computed from MARCS model atmospheres. Hence, the correction $q_b^*(Li)$, computed with the 1D LTE profiles of the 1D LHD models, should be applied to their $^6Li/^7Li$ isotopic ratios. The resulting downward corrections are typically in the range $1\% < q_b^*(Li) < 2\%$ for the stars of their sample (cf. Steffen *et al.* 2010, Fig. 2). After subtracting the individual $q_b^*(Li)$ for each of these stars, according to their T_{eff}, $\log g$, and [Fe/H], the mean $^6Li/^7Li$ isotopic ratio of the sample is reduced from 0.0212 to 0.0056, as illustrated in Fig. 2. Given the $^6Li/^7Li$ isotopic ratios and their 1σ error bars as determined by Asplund *et al.* (2006), the number of stars with a ^6Li detection above the 2σ and 3σ level is 9 and 5, respectively, out of 24. After correction, the number of 2σ and 3σ detections is reduced to 4 and 2, respectively. One of the stars meeting the 3σ criterion after correction, HD 106038, survives only because of its particularly small error bar of ± 0.006. The other one is G020-024, which shows the clearest evidence for the presence of ^6Li ($q(Li) = 0.052 \pm 0.017$), while HD 102200 remains the only clear 2σ detection ($q(Li) = 0.033 \pm 0.013$). The spectra of these stars should be reanalyzed with 3D NLTE line profiles.

4. Analysis of observed spectra: 3D NLTE versus 1D LTE line fitting

As a further exercise, we have fitted the observed Li I $\lambda 6707$ Å spectra of three halo turn-off stars (see Table 2), both with 3D NLTE and 1D LTE synthetic line profiles. Since the parameters of these three stars are very similar, the synthetic spectra were computed in all cases from hydrodynamical model d3t6300g40mm20n01 (see Table 1) and the corresponding 1D LHD model. The standard approach is to vary the four parameters $A(Li)$, $q(Li)$, V_{BR}, and Δv to find the optimum line profile fit, as described above (method I). The results are presented in Table 3. As expected, the 3D analysis yields lower $^6Li/^7Li$ isotopic ratios by about 1.7%. The numbers differ slightly from those given by Steffen *et al.* 2010 due to an upgrade of the line fitting procedure, but the conclusions remain unchanged: HD 74000 and G271−162 are considered non-detections, while HD 84937 remains a clear ^6Li detection with $q^{(3D-NLTE)}(Li) \approx 5\%$.

For completeness, Table 3 also shows the results of fitting the observed lines with 3D LTE synthetic profiles (not recommended). The ^6Li abundances obtained in this way lie between the 3D NLTE and the 1D LTE results. It is not obvious why fitting with the more asymmetric 3D LTE profiles gives higher ^6Li than fitting with the slightly more symmetric 3D NLTE profiles, but this is a robust result.

For HD 74000, we also tried an alternative approach (method II), where V_{BR} is deter-

Table 2. Observed Li I $\lambda 6707$ Å spectra of three metal-poor turn-off stars

Star	T_{eff} [K]	$\log g$	[Fe/H]	R=$\lambda/\Delta\lambda$	S/N	Instrument	Reference
HD 74000	6203	4.03	-2.05	120 000	600	ESO3.6 / HARPS	Cayrel *et al.* 2007
G271−162	6330	4.00	-2.25	110 000	600	VLT / UVES	Nissen *et al.* 2000
HD 84937	6300	4.00	-2.30	100 000	630	CFHT / GECKO	Cayrel *et al.* 1999

Table 3. Fitting the observed spectra of Table 2 with 3D and 1D synthetic line profiles. Columns (4)-(7) show the results for $v \sin i = 0.0$ / 2.0 km/s.

Star	synthetic spectrum	fitting method	A(Li) [1]	n(^{6}Li)/n(^{7}Li) [%]	V_{BR} [2] [km/s]	Δv [km/s]
HD 74000	3D NLTE	I	2.25 / 2.25	**-1.1** / **-1.1**	3.1 / 2.1	0.64 / 0.64
	(3D LTE)	I	1.85 / 1.85	**-0.4** / **-0.5**	4.7 / 4.1	0.66 / 0.67
	1D LTE	I	2.23 / 2.23	**0.6** / **0.6**	5.9 / 5.4	0.43 / 0.43
	3D NLTE	II	2.25 / 2.25	**-1.1** / **-1.3**	**3.1** / **2.2**	0.64 / 0.65
	(3D LTE)	II	1.84 / 1.84	**4.6** / **4.2**	**3.1** / **2.2**	0.46 / 0.47
	1D LTE	II	2.23 / 2.23	**1.7** / **1.7**	**5.6** / **5.1**	0.39 / 0.39
G271−162	3D NLTE	I	2.30 / 2.30	**0.7** / **0.6**	3.7 / 2.9	0.04 / 0.04
	(3D LTE)	I	1.89 / 1.89	**1.3** / **1.1**	5.2 / 4.6	0.06 / 0.07
	1D LTE	I	2.27 / 2.27	**2.3** / **2.4**	6.2 / 5.8	-0.17 / -0.17
HD 84937	3D NLTE	I	2.20 / 2.20	**5.2** / **5.2**	3.3 / 2.4	0.02 / 0.02
	(3D LTE)	I	1.80 / 1.80	**5.8** / **5.7**	4.8 / 4.3	0.05 / 0.05
	1D LTE	I	2.18 / 2.18	**6.9** / **6.9**	6.0 / 5.6	-0.19 / -0.19

Notes: [1] $\log \left[n(^6\text{Li}) + n(^7\text{Li}) \right] - \log n(\text{H}) + 12$; [2] Gaussian kernel, **bold:** fixed from Fe I lines

mined from other spectral lines, and is then fixed during the fitting of the Li I $\lambda 6707$ Å feature. For this purpose, we rely on a set of 6 clean Fe I lines with similar excitation potential between 2.4 and 2.6 eV: the 5 lines of Cayrel *et al.* (2007), Table 1, plus Fe I $\lambda 6230.7$ Å, $E_i = 2.559$ eV. Their equivalent widths range from $W \approx 13$ to 30 mÅ, embracing the strength of the Li doublet. Fitting the 6 Fe I lines with 3D LTE synthetic line profiles, we obtain $V_{BR}(\text{Fe}) = 3.05$ $(2.15) \pm 0.16$ (0.23) km/s for $v \sin i = 0$ (2) km/s, in close agreement with $V_{BR}(\text{Li})$ inferred from the fitting of the Li I profile. This result may be taken as an indication that, in contrast to Li, the selected Fe I lines are not severely affected by departures from LTE. We note, however, a trend of $V_{BR}(\text{Fe})$ increasing slightly with W, which remains to be understood. If instead the Fe I lines are fitted with 1D LTE synthetic profiles, we find $V_{BR}(\text{Fe}) = 5.61$ $(5.13) \pm 0.07$ (0.09) km/s, systematically lower than $V_{BR}(\text{Li})$ by 0.3 km/s. Fixing $V_{BR} = V_{BR}(\text{Fe})$, the best fit of the Li I doublet implies $q^{1\text{D LTE}}(\text{Li}) = 1.7\%$, which is 1.1% higher than with method I. Finally, Table 3 demonstrates that applying method II with 3D LTE fitting of Li I leads to a severe overestimation of the ^{6}Li/^{7}Li isotopic ratio: $q^{3\text{D LTE}}(\text{Li}) > 4\%$ compared to $q^{3\text{D NLTE}}(\text{Li}) = -1.1\%$!

5. Conclusions

The ^{6}Li/^{7}Li isotopic ratio derived from fitting of the Li I doublet with 3D NLTE synthetic line profiles is shown to be about 1% to 2% lower than what is obtained with 1D LTE profiles. Based on this result, we conclude that only 2 out of the 24 stars of the Asplund *et al.* (2006) sample would remain significant ^{6}Li detections when subjected to a 3D non-LTE analysis, suggesting that the presence of ^{6}Li in the atmospheres of galactic halo stars is rather the exception than the rule, and hence does not necessarily constitute a *cosmological* ^{6}Li problem. If we adopt the approach by Asplund *et al.* (2006), relying on additional spectral lines to fix the residual line broadening, the difference between 3D NLTE and 1D LTE results increases even more, as far as we can judge from our case study HD 74000. Until the 3D NLTE effects are fully understood for all involved lines, we consider this method as potentially dangerous.

References

Asplund, M., Lambert, D. L., Nissen, P. E., Primas, F., & Smith, V. V. 2006, *ApJ*, 644, 229
Barklem, P.S., Belyaev, A.K., Asplund, M. 2003, *A&A*, 409, L1
Castelli, F., & Kurucz, R. L. 2004, arXiv:astro-ph/0405087

Cayrel, R., Spite, M., Spite, F., Vangioni-Flam, E., Cassé, M., Audouze, J. 1999, *A&A*, 343, 923

Cayrel, R., Steffen, M., Chand, H., Bonifacio, P., Spite, M., Spite, F., Petitjean, P., Ludwig, H.-G., & Caffau, E. 2007, *A&A*, 473, L37

Cayrel, R., Steffen, M., Bonifacio, P., Ludwig, H.-G., Caffau, E. 2008, *Nuclei in the Cosmos (NIC X)*, availale online at http://adsabs.harvard.edu/abs/2008nuco.confE...2C

Christlieb, N. 2008, *Journal of Physics G: Nuclear Physics*, 35, 014001

Freytag, B., Steffen, M., & Dorch, B. 2002, *AN*, 323, 213

Ludwig, H.-G., Caffau, E., Steffen, M., Freytag, B., Bonifacio, P., & Kučinskas, A. 2009, *MemSAI*, 80, 708

Nissen, P.E., Asplund, M., Hill, V., D'Odorico, S. 2000, *A&A* 357, L49

Sbordone, L., Bonifacio, P., Caffau, E., *et al.* 2009, *A&A* (in press)

Steffen, M., Cayrel, R., Boinfacio, P., Ludwig, H.-G., Caffau, E. 2010, in: K. Cunha, M. Spite, and B. Barbuy (eds.) *Chemical Abundances in the Universe: Connecting First Stars to Planets*, Proc. IAU Symposium No. 265, (in press, http://arxiv.org/abs/0910.5917v1)

Wedemeyer, S., Freytag, B., Steffen, M., Ludwig, H.-G., & Holweger, H. 2004, *A&A*, 414, 1121